Elastic moduli of hexagonal diamond and cubic diamond formed under shock compression

Travis J. Volz and Y. M. Gupta

Phys. Rev. B **103**, L100101 — Published 8 March 2021

DOI: 10.1103/PhysRevB.103.L100101

Elastic moduli of hexagonal diamond and cubic diamond formed under shock compression

Travis J. Volz* and Y. M. Gupta†

Institute for Shock Physics and Department of Physics and Astronomy, Washington State University, Pullman, Washington 99164, USA

(Received 29 January 2021)

The relative stiffnesses and strengths of hexagonal diamond and cubic diamond constitute long standing unresolved issues, because relevant experimental results are lacking. Laser interferometry was used to experimentally determine the longitudinal sound speeds and moduli in hexagonal diamond and cubic diamond formed during the shock compression of graphite. The hexagonal diamond longitudinal moduli are significantly larger than the cubic diamond longitudinal moduli, and even exceed averaged cubic diamond single crystal values. The measured hexagonal diamond longitudinal moduli, combined with high-pressure bulk moduli for cubic diamond single crystals, show that shock-formed hexagonal diamond shear moduli are larger than the shear moduli for cubic diamond single crystals.

Cubic diamond, the hardest known bulk solid, has long been an important material for scientific and technological applications because of its exceptional mechanical, optical, and thermal properties [1]. Due to the considerable interest in the utility of extremely hard and strong materials, significant scientific effort has been devoted to discovering and characterizing solids

* Present address: Dynamic Compression of Materials Group, Lawrence Livermore National Laboratory, Livermore, CA 94550.

† Corresponding author. ymgupta@wsu.edu.

with mechanical properties superior to those of cubic diamond [2–4]. Hexagonal diamond, a candidate material, was first discovered in meteorites [5,6] and synthesized in the laboratory [7] in 1967. Hexagonal diamond, similar to cubic diamond, is comprised entirely of tetragonally bonded carbon atoms with comparable bond lengths and bulk density [7]. Because of its potential for achieving superior mechanical properties, hexagonal diamond has long been considered as an excellent alternative to cubic diamond. However, to date, hexagonal diamond mechanical properties have been examined almost exclusively using computational methods, due to the lack of available macroscopic samples for experimental measurements [8].

Computational studies have reported that hexagonal diamond is stronger [9], stiffer [10], and has larger elastic moduli than cubic diamond [11], despite computations also suggesting that hexagonal diamond is thermodynamically less stable [12,13]. One computational study [9], utilizing first-principles total energy calculations, reported that the ideal indentation strength of hexagonal diamond surpasses that of cubic diamond by 58%. However, indentation hardness results are extremely difficult to assess as they are strongly dependent on the testing conditions imposed [14]. We note that claims of materials exhibiting hardnesses significantly greater than cubic diamond values have been rebutted strongly and deemed scientifically unreliable in a recent article [14], which also provides an extensive list of references regarding this topic.

Although the calculated [11–13] and experimentally determined [15] hexagonal diamond bulk modulus values (measure of volume incompressibility) are comparable to the bulk modulus of cubic diamond [16], experimental evidence to support claims of superior strength and/or hardness – which are governed by the shear modulus [17] – is lacking for hexagonal diamond. Simply stated, the bulk modulus is not a measure of material strength and hardness – properties that govern a material's ability to resist deformation. Hence, experimental determination of

hexagonal diamond's longitudinal and/or shear modulus constitutes an important need to evaluate its inherent mechanical strength and to make meaningful comparisons with cubic diamond moduli.

Hexagonal diamond formation has been reported in samples recovered near meteorite impacts [5,18], from shock compression experiments [19], and from static compression experiments [7,15]. However, careful reanalyses [8,20] of the so-called hexagonal diamond samples and x-ray diffraction (XRD) data from the earlier studies revealed that the previously reported hexagonal diamond is more accurately characterized as stacking disordered cubic diamond with some cubic and hexagonal stacking of the carbon layers. One study reported that previous samples contained, at most, ~60% hexagonal stacking [20], but another study claimed to exceed this threshold [21]. The above contradictory findings demonstrate that the use of recovered samples for measuring hexagonal diamond properties is questionable.

Unlike recovery studies, recent *in situ* XRD measurements have definitively established the formation of hexagonal diamond during shock compression of highly oriented pyrolytic graphite [22,23]. In these shock experiments, the hexagonal diamond was formed during uniaxial strain compression. This feature avoids the complex thermomechanical unloading histories and the resulting challenges associated with recovered samples [20,24]. However, determination of the hexagonal diamond properties formed under shock compression [22,23] requires *in situ* measurements while the material is in the shock compressed state – the focus of the present work.

We present results from plate impact experiments that provide the longitudinal moduli of hexagonal and cubic diamond formed during the shock compression of three graphite types. Using the front-surface impact method [25–28], longitudinal sound speeds were measured in the shock compressed state. These measurements along with the densities in the shocked state provided the longitudinal moduli for both diamond types formed under shock compression. Our experimental

results show unequivocally that the hexagonal diamond longitudinal moduli are significantly higher than the cubic diamond moduli, and even exceed ambient single crystal cubic diamond longitudinal moduli by a considerable amount.

Figure 1(a) shows the configuration used in our front-surface impact experiments. Three graphite types, obtained from Momentive Performance Materials, were studied: ZYB-grade highly oriented pyrolytic graphite (HOPG), ZYH-grade HOPG, and as-deposited pyrolytic graphite (PG). Each graphite sample was nominally ~1 mm thick, 10 mm in diameter (one experiment used a 20 mm diameter sample), and the average crystallite *c*-axis was oriented perpendicular to the sample face. Graphite samples, bonded to Lexan (polycarbonate) projectiles, were accelerated to impact velocities between 4.1 and 7.2 km/s using a two-stage light-gas gun and impacted onto [100] oriented lithium fluoride (LiF) optical windows. The LiF windows had gold mirrors vapor-deposited on the diffuse impact faces to enable interface velocity measurements using both VISAR [29] and PDV [30] diagnostics. The sample and window dimensions were chosen to ensure that the sound speed measurements would be obtained during uniaxial strain compression. Further experimental details, including material characterization, are reported in the Supplemental Material (SM) [31].

Figure 1(b) shows schematically the shock and release wave propagation for the front-surface impact experiments, and Fig. 1(c) shows the corresponding particle velocity profile at the sample/LiF interface. Upon impact (t_0), shock waves propagate into the graphite and LiF, resulting in a jump in the interface particle velocity. The measured particle velocity, u_{peak}, in the LiF [36] provides the peak stress in each experiment. Peak longitudinal stresses between 34 and 83 GPa were obtained in the present work, resulting in the formation of hexagonal diamond and cubic diamond [22,23] from the shock compression of HOPG and PG, respectively.

Determination of the stresses, densities, longitudinal sound speeds, and corresponding longitudinal moduli in the shocked state – from the measured particle velocity histories (Fig. 2) – is based on well-established analytical procedures [25–28] and the same are presented in the SM [31]. Before describing the experimental results, a brief overview of the overall approach – utilizing Fig. 1 – is summarized. At t_0, a shock wave with velocity, U_s, propagates into the graphite sample and produces the high stress state that transforms the graphite into diamond; in all our experiments the shock wave amplitudes were well above the transformation stresses for HOPG and PG [22,23,35]. Subsequently, the propagating shock reflects from the sample/Lexan interface as a longitudinal release wave which unloads the peak stress in the shock compressed state. The leading edge of the longitudinal release propagates back at the isentropic Lagrangian sound speed in the peak state [24-27], $c_{L,L}$ – corresponding to the sound speed in the diamond phase. The release wave arrival at the diamond/LiF interface (t_{rel}), the ambient sample thickness (h_0), and the shock velocity provide the longitudinal sound speed in the shocked state (diamond):

$$t_{rel} - t_0 = \frac{h_0}{U_S} + \frac{h_0}{c_{L,L}} \tag{1}$$

In only one experiment (34 GPa peak stress), two waves propagated into the graphite because the first wave corresponding to the phase transformation onset was not overdriven [35]. A slightly modified analysis method, described in the SM [31], was used for this experiment.

We note that the determination of $c_{L,L}$ is quite sensitive to small changes in t_{rel}. For example, for a 1 mm sample, with $U_S = 8.5$ km/s and $t_{rel} = 150$ ns (values comparable to our experiments), a 1 ns difference in t_{rel} results in a 3% difference in $c_{L,L}$. For this reason, great care was taken to ensure the accuracy of t_{rel}. As described in detail in the SM [31] (see Fig. S3(b)), t_{rel} was determined from the intersection of lines fit to the peak state particle velocity before release and to the initial portion of the release. Although a range of fitting assumptions gave very

consistent results (less than 0.4 ns differences), each t_{rel} determination was also cross-validated using the two independent velocity measurements (VISAR and PDV) for each experiment, which gave very consistent results.

Particle velocity profiles measured at the sample/LiF interface for all eight experiments are shown in Fig. 2; to facilitate comparisons between the profiles, time after impact was normalized by the ambient sample thickness. Overall, the measured profiles – apart from the fluctuations discussed below – are very similar to the idealized profile shown in Fig. 1(c). Despite the observed fluctuations, the release wave arrivals were very distinct and permitted precise determination (within ~1 ns) of the release time (t_{rel}) in our experiments. The following general pattern was observed in all eight experiments: the peak state durations were shorter for experiments having higher peak stresses (corresponding to higher interface velocities in Fig. 2). This result is expected due to a combination of faster shock velocities and faster longitudinal release arrival at higher stresses.

Given the heterogenous nature of the starting graphite samples – for both HOPG types and PG – some level of fluctuations was expected in the impact surface measurements. In addition, because the samples are commercially processed, with variability in material parameters likely between samples, some scatter in the velocity histories and results between experiments is not unreasonable. The measured profiles in Fig. 2 show that the fluctuations in the transformed material are more pronounced for the PG than for the HOPG. Although we cannot be certain [32], these differences likely reflect the heterogenous nature (and orientational order) of the cubic diamond and hexagonal diamond formed under shock compression. As noted in the SM (Fig. S1), the mosaic spreads for the PG samples were more than an order of magnitude higher than the HOPG samples.

To aid the analysis and discussion of the sound speed measurements, we briefly summarize our earlier findings [22,23,35] relevant to the present work. Both HOPG types transform to hexagonal diamond above 22 GPa and the PG transforms to cubic diamond above 46 GPa; the transformation to the diamond phases are completed in a few nanoseconds. Within experimental uncertainties, the longitudinal stress – density Hugoniots of both hexagonal diamond and cubic diamond – formed under shock compression – are nearly identical and are in good agreement with the elastic Hugoniot data obtained from the shock compression of bulk cubic diamond single crystals [38]. Although *in-situ* x-ray diffraction data showed that both shock-formed diamond types consisted of polycrystalline aggregates, the cubic diamond consisted of nearly randomly oriented nanograins ($\gtrsim 5$ nm) and the hexagonal diamond consisted of larger grains with significant texture (hexagonal diamond $[10\bar{1}0]$ along shock loading direction).

The longitudinal Lagrangian sound speeds, obtained using Eq. (1) for all experiments, are listed in the SM (Table S2); other relevant continuum quantities corresponding to the shocked state are also listed in that Table. As noted above, small variations between experiments contribute to some scatter in the results, as determined from Eq. (1). After accounting for the sample thickness change due to compression, Eulerian sound speeds were obtained from the Lagrangian sound speeds and the same are plotted versus the peak longitudinal stress in Fig. 3. In addition, sound speeds for the graphite phase [27] (below transformation) and results from an earlier study [39] on shock compressed PG are also shown. The average of the hexagonal diamond sound speeds (~20 km/s) is significantly larger than the cubic diamond average (~18 km/s), even leaving aside the lowest value from Exp. 5. Determination of the error bars in our results are described in the SM. No explanation of the error bar determination for in the results from Ref. [39] was provided in that paper and the error bars for Ref. [27] are on the scale of the symbols.

For comparison purposes, we show several reference results in Fig. 3, corresponding to ambient cubic diamond and hexagonal diamond sound speeds. The first is the longitudinal sound speed along the [100] direction for single crystal cubic diamond. Because cubic diamond is not an isotropic solid and because the shock-formed diamonds in our work are polycrystalline solids, we also show the orientationally averaged ambient longitudinal sound speeds using Voigt and Reuss averages [40]; the two averages are very close (18.17 km/s and 18.03 km/s, respectively). Due to the incompressibility of cubic diamond, the sound speeds should not vary much over the stress range shown. In addition to the cubic diamond reference results, we also show the ambient hexagonal diamond longitudinal sound speed expected from an average [22] of theoretically calculated second order elastic constants along hexagonal diamond $[10\bar{1}0]$, the crystallite orientation observed in the XRD experiments [22,23]. The calculated ambient hexagonal diamond sound speed (18.7 km/s) is larger than all cubic diamond elastic sound speeds and is consistent with the pattern observed from the experimental results in Fig. 3 – the longitudinal sound speeds in hexagonal diamond are measurably larger than the cubic diamond sound speeds shown.

Using the density (ρ_1) and the Eulerian sound speed ($c_{L,E}$) in the shocked state, the longitudinal moduli in the shock-formed hexagonal diamond and cubic diamond are given by

$$L = \rho_1 \, c_{L,E}^2. \tag{2}$$

In Fig. 4, we have plotted the longitudinal elastic modulus – for both shock-formed hexagonal diamond and cubic diamond – as a function of the peak stress. For reference, we show the longitudinal modulus values for the graphite phase (at stresses below the transformation stress) and bulk cubic diamond. Using the second and third order elastic constants for cubic diamond [41], we show the longitudinal elastic modulus for shock wave compression along the [100] direction. Since Voigt and Reuss averages have been reliably established only for second order elastic

constants [40], the polycrystalline averages shown in Fig. 4 were obtained using ambient sound speeds (shown in Fig. 3) and the densities in the shocked state; hence, the increase in the longitudinal modulus values with the longitudinal stress.

Figure 4 highlights notable findings from the present work. These results show that the longitudinal moduli for shock-formed hexagonal diamond (from HOPG) are significantly larger than the corresponding moduli (1120 – 1350 GPa, even discounting the 840 GPa value) for shock-formed cubic diamond (from PG) and the moduli for bulk single crystals and polycrystalline cubic diamond. The blue line – shown as a visual guide – emphasizes the trend in hexagonal diamond moduli relative to the cubic diamond moduli. Because the shock-formed hexagonal diamond has a strong preferred orientation with the hexagonal diamond $[10\bar{1}0]$ axis along the loading direction [22,23], comparing the present results to the effective moduli along the hexagonal diamond $[10\bar{1}0]$ is useful. This value (1230 GPa), reported in Ref. [22] and shown as an intercept of the blue line, corresponds to the average theoretical modulus along hexagonal diamond $[10\bar{1}0]$. Although previous theoretical work [10] has suggested that hexagonal diamond is stiffer than cubic diamond, the present work provides the first experimental demonstration of the stiffer response of hexagonal diamond. A comparison of the graphite and hexagonal diamond longitudinal moduli in Fig. 4 shows a dramatic change across the phase transition – nearly a 7-fold increase between the modulus at 18 GPa (graphite phase, prior to the transformation) and 34 GPa (diamond phase, after the transformation). We also note that the experimentally measured longitudinal moduli for shock-formed cubic diamond (from PG) are generally consistent with the well-established longitudinal moduli for single crystal and polycrystalline cubic diamond.

Although the present experiments only provide a direct experimental determination of the hexagonal diamond longitudinal modulus, the hexagonal diamond shear modulus can be estimated

using the following approximate approach. We first recall the definition of the longitudinal modulus (L) in terms of the bulk (K) and shear (G) moduli:

$$L = K + \frac{4}{3}G. \tag{3}$$

Because both cubic and hexagonal diamond are carbon allotropes, have similar bonding, and have comparable densities, their bulk moduli are expected to be similar. Indeed, both computational [11–13] and experimental [15] studies have established the similarity of hexagonal diamond and cubic diamond bulk moduli. The ambient hexagonal diamond bulk modulus (425 GPa) – experimentally determined through *in*-situ XRD measurements of the unit cell [15] – is somewhat comparable to the cubic diamond value of 445 GPa [14]. Next, we use the bulk modulus values of cubic diamond single crystals at 60 and 80 GPa longitudinal stresses — determined from averaging nonlinear elastic constants [41] for [100], [110], and [111] orientations — as a substitute for the shock-formed hexagonal diamond bulk modulus values at these stresses since the same have not been determined experimentally. Using these substitute bulk moduli, the hexagonal diamond longitudinal moduli measured in the present work (blue line in Fig. 4) and Eq. (3), we obtained the following results. The shock-formed hexagonal diamond shear moduli are at least 8 to 13 percent higher than the corresponding shear moduli for bulk cubic diamond crystals at 60 and 80 GPa, respectively. These differences represent lower bounds because the shock-formed hexagonal diamonds are at higher temperatures and the substitute bulk moduli used are likely larger than the actual hexagonal diamond values (based on a comparison of the ambient bulk modulus values listed above).

Due to the approximations noted in the paragraph above – resulting from the lack of bulk modulus measurements for both shock-formed hexagonal diamond and cubic diamond – it is difficult to assign meaningful error bars to the shear modulus values for shock-formed hexagonal

diamond. Hence, the 8 to 13 percent difference between the inferred shear modulus values for shock-formed hexagonal diamond and bulk single crystal cubic diamond should be viewed in a qualitative manner.

Using front-surface impact experiments on highly oriented pyrolytic graphite (HOPG) and as-deposited pyrolytic graphite (PG), at stresses above their respective phase transformation stresses, the longitudinal moduli of shock-formed hexagonal diamond and cubic diamond were experimentally measured – thus, addressing a long-standing scientific need. Our results show that the longitudinal modulus of shock-formed hexagonal diamond is significantly larger than that of shock-formed cubic diamond and even single crystal cubic diamond. By treating the hexagonal diamond bulk modulus variations with compression to be similar to that of averaged cubic diamond single crystal variations with compression and using the longitudinal moduli of hexagonal diamond measured in this work, we infer the shear modulus of hexagonal diamond to be at least 8 – 13 percent larger than the corresponding cubic diamond shear moduli. This difference – admittedly, a qualitative measure because of the lack of bulk modulus measurements – can be put in perspective by noting the following comment from Ref. [14]: "In contrast to the bulk modulus, reports on the shear moduli above the diamond value are almost absent in both experimental and theoretical works."

Because the strength and hardness of a defect-free crystalline solid are determined by its shear modulus [14,17], our results provide the first experimental evidence that perfect hexagonal diamond crystals are stronger and harder than perfect cubic diamond crystals. Of course, the strength of a real crystal will depend on both the shear modulus and the density of defects in the crystal [17]. Nevertheless, the present work will provide an impetus to explore the production of hexagonal diamonds – an ultrahard material for use in numerous technological applications.

Nate Arganbright, Kurt Zimmerman, and Yoshi Toyoda are sincerely thanked for their assistance with the front-surface impact experiments. Drs. Surinder Sharma, Stefan Turneaure, Michael Winey, and Pritha Renganathan are thanked for useful discussions related to the graphite to diamond transformation, high-pressure phases obtained in these experiments, and analysis. Discussions with Michael Winey regarding cubic diamond elastic moduli are gratefully acknowledged. This Letter is based upon work supported by the U. S. Department of Energy (DOE), National Nuclear Security Administration (NNSA) under Award Nos. DE-NA0002007 and DE-NA0003957. Parts of this manuscript were finalized under the auspices of the U.S. Department of Energy (DOE) at Lawrence Livermore National Laboratory under Contract No. DE-AC52-07NA27344.

Figures

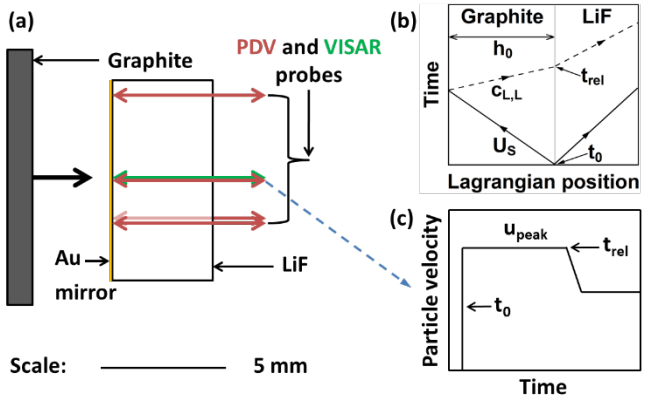

FIG. 1. Front-surface impact experimental approach. (a) Experimental configuration. (b) An $h-t$ plot showing wave propagation. Solid lines indicate shock waves and dashed lines indicate release waves. (c) Idealized center probe particle velocity history obtained at the graphite/LiF interface.

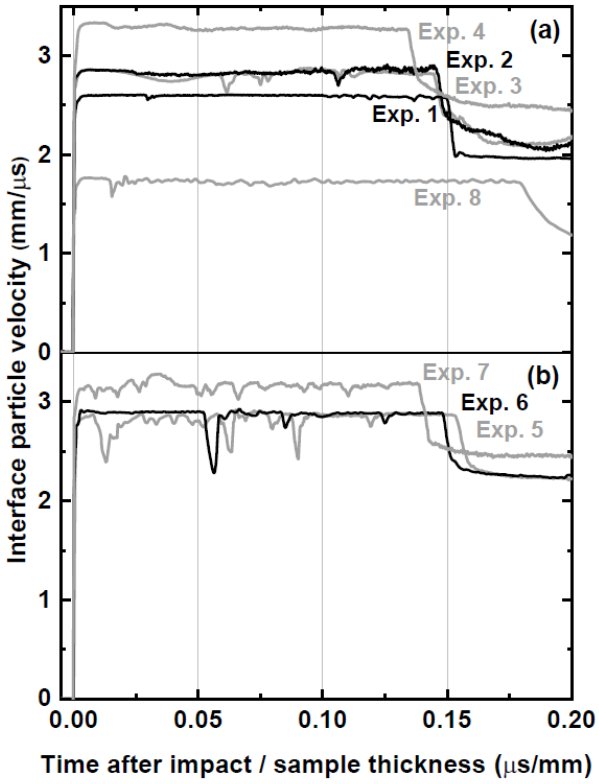

FIG. 2. Particle velocity histories obtained at the graphite/LiF interface for HOPG (a) and PG (b). Experiments 1–4 are on ZYB-grade HOPG and experiment 8 is on ZYH-grade HOPG. The particle velocity history for Exp. 6 utilized PDV measurements due to VISAR contrast loss. All other profiles were obtained from VISAR measurements.

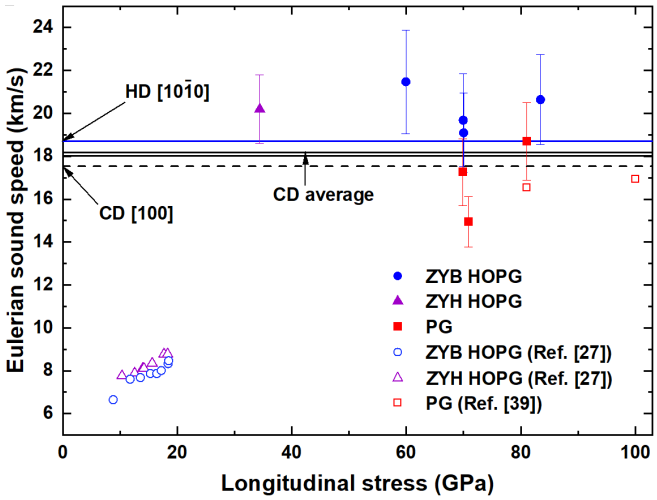

FIG. 3. Eulerian sound speeds. Sound speeds determined for each experiment are shown as solid symbols and previous sound speeds reported for shock compressed HOPG [27] and PG [39] are shown as open symbols. For comparison with the experimental results, the dashed line shows ambient cubic diamond (CD) sound speed along the [100] orientation and the solid black lines show the ambient sound speeds corresponding to the Voigt (upper bound) and Reuss (lower bound) averaged CD elastic moduli. The ambient hexagonal diamond (HD) sound speed calculated from an average [22] of theoretical elastic constants along the orientation observed in XRD experiments ([10$\bar{1}$0]) is shown as a blue line.

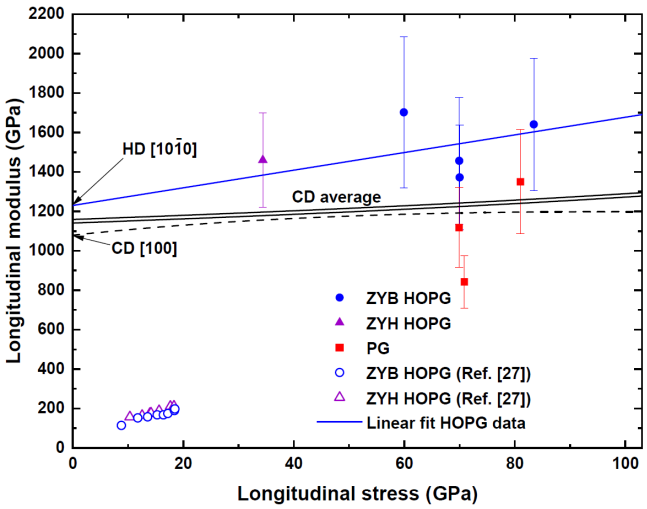

FIG. 4. Longitudinal moduli. Experimentally determined diamond moduli are shown as solid symbols and moduli reported for HOPG below the transition [27] are shown as open symbols. For comparison with the present experimental results, the dashed line shows cubic diamond (CD) [100] moduli calculated from second and third order elastic constants. Solid lines show the moduli corresponding to the Voigt (upper) and Reuss (lower) averaged CD elastic moduli scaled with increasing stress (and hence density) assuming a linear elastic response. The blue line is a linear fit for visual reference, with the intercept fixed at the ambient hexagonal diamond (HD) modulus along $[10\bar{1}0]$, calculated from an average [22] of theoretical elastic constants.

References

[1] J. E. Field, editor , *The Properties of Natural and Synthetic Diamond* (Academic Press, Inc., San Diego, CA, 1992).

[2] A. Y. Liu and M. L. Cohen, Science **245**, 841 (1989).

[3] D. M. Teter and R. J. Hemley, Science **271**, 53 (1996).

[4] H. Niu, X. Q. Chen, S. Wang, D. Li, W. L. Mao, and Y. Li, Phys. Rev. Lett. **108**, 135501 (2012).

[5] R. E. Hanneman, H. M. Strong, and F. P. Bundy, Science **155**, 995 (1967).

[6] C. Frondel and U. B. Marvin, Nature **214**, 587 (1967).

[7] F. P. Bundy and J. S. Kasper, J. Chem. Phys. **46**, 3437 (1967).

[8] P. Nemeth, L. A. J. Garvie, T. Aoki, N. Dubrovinskaia, L. Dubrovinsky, and P. R. Buseck, Nat. Commun. **5**, 5447 (2014).

[9] Z. Pan, H. Sun, Y. Zhang, and C. Chen, Phys. Rev. Lett. **102**, 055503 (2009).

[10] L. Qingkun, S. Yi, L. Zhiyuan, and Z. Yu, Scr. Mater. **65**, 229 (2011).

[11] E. Güler and M. Güler, Appl. Phys. A Mater. Sci. Process. **119**, 721 (2015).

[12] S. Fahy and S. G. Louie, Phys. Rev. B **36**, 3373 (1987).

[13] B. Wu and J. Xu, Phys. Rev. B **57**, 13355 (1998).

[14] V. V. Brazhkin and V. L. Solozhenko, J. Appl. Phys. **125**, 130901 (2019).

[15] T. Yagi, W. Utsumi, M. A. Yamakata, T. Kikegawa, and O. Shimomura, Phys. Rev. B **46**, 6031 (1992).

[16] H. J. McSkimin, P. Andreatch, and P. Glynn, J. Appl. Phys. **43**, 985 (1972).

[17] A. Kelly and N. H. MacMillan, *Strong Solids*, 3rd ed. (Clarendon Press, Oxford, England, 1986).

[18] R. S. Clarke Jr, D. E. Appleman, and D. R. Ross, Nature **291**, 396 (1981).

[19] L. F. Trueb, J. Appl. Phys. **39**, 4707 (1968).

[20] C. G. Salzmann, B. J. Murray, and J. J. Shephard, Diam. Relat. Mater. **59**, 69 (2015).

[21] T. B. Shiell, D. G. McCulloch, J. E. Bradby, B. Haberl, R. Boehler, and D. R. McKenzie, Sci. Rep. **6**, 37232 (2016).

[22] S. J. Turneaure, S. M. Sharma, T. J. Volz, J. M. Winey, and Y. M. Gupta, Sci. Adv. **3**, eaao3561 (2017).

[23] T. J. Volz, S. J. Turneaure, S. M. Sharma, and Y. M. Gupta, Phys. Rev. B **101**, 224109 (2020).

[24] F. P. Bundy, W. A. Bassett, M. S. Weathers, R. J. Hemley, H. K. Mao, and A. F. Goncharov, Carbon N. Y. **34**, 141 (1996).

[25] T. S. Duffy and T. J. Ahrens, J. Appl. Phys. **82**, 4259 (1997).

[26] B. J. Jensen, F. J. Cherne, J. C. Cooley, M. V. Zhernokletov, and A. E. Kovalev, Phys. Rev. B **81**, 214109 (2010).

[27] M. Lucas, J. M. Winey, and Y. M. Gupta, J. Appl. Phys. **118**, 245903 (2015).

[28] E. J. Berryman, J. M. Winey, Y. M. Gupta, and T. S. Duffy, Geophys. Res. Lett. **46**, 13695 (2019).

[29] L. M. Barker and R. E. Hollenbach, J. Appl. Phys. **43**, 4669 (1972).

[30] O. T. Strand, D. R. Goosman, C. Martinez, T. L. Whitworth, and W. W. Kuhlow, Rev. Sci. Instrum. **77**, 083108 (2006).

[31] See Supplemental Material at https://??? for additional details regarding material characterizations, experimental configurations, and analysis, including Refs. [32-37].

[32] T. J. Volz, Ph.D. dissertation, Washington State University, 2020.

[33] J. F. Green, P. Bolsaitis, and I. L. Spain, J. Phys. Chem. Solids **34**, 1927 (1973).

[34] M. Lucas, J. M. Winey, and Y. M. Gupta, J. Appl. Phys. **114**, 093515 (2013).

[35] T. J. Volz and Y. M. Gupta, J. Appl. Phys. **125**, 245902 (2019).

[36] P. A. Rigg, M. D. Knudson, R. J. Scharff, and R. S. Hixson, J. Appl. Phys. **116**, 033515 (2014).

[37] R. G. McQueen and S. P. Marsh, J. Appl. Phys. **31**, 1253 (1960).

[38] J. M. Lang Jr. and Y. M. Gupta, Phys. Rev. Lett. **106**, 125502 (2011).

[39] J. Shaner, J. Brown, C. Swenson, and R. Mcqueen, J. Phys. **45**, 235 (1984).

[40] D. N. Blaschke, J. Appl. Phys. **122**, 145110 (2017).

[41] J. M. Winey, A. Hmiel, and Y. M. Gupta, J. Phys. Chem. Solids **93**, 118 (2016).